DOI 10.24425/aee.2026.158262

Terahertz identification method for core rods fracture of composite insulators

PIN JIANG[1], YANYAN BAO[2], YUSHUO WU[2], PEI WANG[2], RUIXUAN LIU[2], XINGYUAN CHEN[1], XIN ZHI[3], SHUAI BING LI[4]✉

[1]*State Grid Gansu Electric Power Company Ultra-High Voltage Company China*

[2]*State Grid Gansu Electric Power Company Electric Power Science Research Institute China*

[3]*School of Automation and Electrical Engineering, Lanzhou Jiaotong University China*

[4]*Shool of New Energy and Power Engineering, Lanzhou Jiaotong University China*

e-mail: {2029707954/1076453621/2665881722/1656714728}@qq.com {wangziai2001/15869118069/17863933067/✉ lishuaibing1105}@163.com

(Received: 09.12.2025, revised: 28.04.2026)

Abstract: Composite insulator mandrels in high-voltage transmission systems are subjected to coupled electro-thermal-mechanical stresses, making them susceptible to internal fracture damage that threatens grid safety. Traditional detection techniques exhibit significant limitations in early fracture identification, deep defect localization, and quantitative damage assessment. This paper proposes a terahertz identification method for composite insulator mandrel fractures based on terahertz time-domain spectroscopy (THz-TDS), systematically elucidating the electromagnetic response mechanisms and multi-dimensional feature extraction strategies for fracture defects. Transmission-mode non-destructive testing was performed on glass fiber reinforced epoxy resin (GFRP) mandrel specimens in the 0.1–2.5 THz frequency range using a CCT-1800 THz-TDS system. The research reveals: 1) The dielectric discontinuity interface induced by mandrel fractures alters terahertz wave propagation paths, generating distinctive frequency-domain energy spectrum characteristics in the 0.1–0.75 THz band, with significant transmitted energy attenuation in fractured regions; 2) Through multi-frequency comparative analysis, 0.458 THz was determined as the optimal characteristic frequency for fracture boundary identification, demonstrating superior imaging contrast and spatial resolution compared to 0.568 THz; 3) Time-domain pulse wave-form analysis indicates that multiple reflection effects at fracture interfaces enhance negative peak amplitudes and peak delays, with peak-to-peak imaging enabling precise

© 2026. The Author(s). This is an open-access article distributed under the terms of the Creative Commons Attribution-NonCommercial-NoDerivatives License (CC BY-NC-ND 4.0, https://creativecommons.org/licenses/by-nc-nd/4.0/), which permits use, distribution, and reproduction in any medium, provided that the Article is properly cited, the use is non-commercial, and no modifications or adaptations are made.

fracture localization. The established two-dimensional integrated diagnostic system of "frequency-domain energy spectrum differential qualitative identification and time-domain waveform characteristic quantitative assessment" provides a novel technical approach for condition monitoring and preventive maintenance of composite insulators in power systems, offering significant engineering application value for ensuring safe and reliable operation of high-voltage transmission lines.

Key words: composite insulator, frequency-domain energy spectrum, mandrel fracture detection, non-destructive testing technology, terahertz time-domain spectroscopy, time-domain waveform analysis

1. Introduction

Composite insulators, as key equipment in power systems, play a critical role in the safe and stable operation of transmission lines. Among them, the core rod, as the central load-bearing component of the composite insulator, primarily bears mechanical loads and provides insulation performance. Its structural integrity is directly related to the reliability of the entire insulator and even the transmission system [1]. However, during long-term operation, the composite insulator core rod is subjected to the coupling effects of various factors such as electric field stress, mechanical stress, and environmental stress, which can lead to internal defects such as micro-cracks and fiber fractures, potentially developing into severe fracture failures. This may result in line outages or even large-scale power failures [2].

At present, the detection of defects in composite insulator core rods mainly relies on traditional methods such as visual inspection, X-ray inspection, and ultrasonic testing [3]. Infrared thermography is highly sensitive to faults such as abnormal temperature rise but has poor detection performance for deep internal defects and early-stage defects that do not show obvious thermal effects. Moreover, it is greatly affected by external environmental conditions, has low signal-to-noise ratios, and is prone to missed detection, which limits the flexibility and timeliness of detection. X-ray inspection can directly obtain images of internal structures, but it is expensive, bulky, time-consuming, and involves radiation risks, which are harmful to the human body and difficult to promote for large-scale use in power grid field operations. Ultrasonic testing is influenced by material inhomogeneity and complex geometries, leading to insufficient accuracy and reliability [4–6]. These methods have significant limitations in early fracture identification, quantitative assessment, and field application, creating an urgent need for new non-destructive testing technologies.

Terahertz technology, as an emerging non-destructive testing method, offers unique advantages such as a wide spectral range, strong penetration ability, and sensitivity to dielectric materials. It has shown great potential in the detection of composite material defects [7]. In recent years, the application research of THz technology in electrical equipment insulation testing has become increasingly active. Studies have shown that THz waves can effectively detect delamination defects, moisture distribution, and aging states of insulating materials [8, 9]. For instance, Li *et al*. [10] proposed a THz intelligent detection method based on the CEEMD-GRU algorithm, achieving high-precision identification and imaging of composite insulator interface defects, with a detection accuracy of 99.25%. Hu *et al*. [11] combined THz time-domain spectroscopy with power spectral density integral imaging, homomorphic filtering, and the Otsu algorithm to develop a high-precision, efficient system for characterizing black silicone rubber cavity defects, enabling

precise imaging and quantitative analysis of the defects. By analyzing changes in frequency domain parameters such as transmittance, extinction coefficient, dielectric loss, and refractive index, qualitative identification, and quantitative assessment of internal defects in insulating materials can be achieved [12].

The detection mechanism is firmly grounded in electromagnetic theory: when terahertz waves encounter the GFRP-air interface at a fracture, the large dielectric constant mismatch ($\varepsilon_r \approx 4-5$ for GFRP vs $\varepsilon_r \approx 1$ for air) creates strong reflection ($R \approx 0.36$ at normal incidence) and transmission coefficient changes according to Fresnel equations (Eqs. 2, 3). This theoretical prediction of energy contrast matches our experimental observations and demonstrates that dielectric discontinuity is a well-established physical mechanism for non-destructive testing.

However, current THz detection technologies are primarily focused on areas such as cable terminals and transformer insulation [13, 14], and Research on the terahertz identification method for fractures in composite insulator cores is still in its early stages. The fiber-reinforced composite material structure, complex stress states, and fracture mechanisms of composite insulator core rods present new technical challenges for fracture identification [15–17]. Therefore, developing a THz-based fracture identification method for composite insulator core rods is of significant theoretical and practical value for improving the reliability of power system operations.

This paper aims to establish a non-destructive fracture identification method for composite insulator core rods based on THz technology [18]. The main innovations include:

1. Establishing the THz response mechanism for fracture defects in core rods. By designing GFRP core rod test samples with different fracture forms, the impact of fracture-induced dielectric discontinuities on the propagation characteristics of THz waves was revealed, and the mechanisms of frequency-domain energy spectrum and time-domain waveform characteristic parameter variations were clarified, providing a theoretical basis for fracture identification;
2. Proposing a fracture identification strategy based on multi-scale THz feature fusion. In the frequency domain, qualitative criteria for the energy spectrum difference in the 0.1–0.75 THz frequency band and the optimal feature frequency of 0.458 THz were established. In the time domain, a quantitative evaluation index system based on negative peak amplitude and peak-to-peak value was constructed. Frequency-domain and time-domain complementary analysis significantly improved the accuracy of fracture location identification and the reliability of severity assessment;
3. Verifying the feasibility of THz transmission detection technology in the composite insulator field. Experimental results show that the established detection method can effectively distinguish normal areas from fractured areas, and the imaging results are intuitive and clear, laying a technological foundation for the development of on-site online monitoring systems.

2. Experimental design

2.1. The fundamental principles of terahertz wave propagation

THz waves refer to electromagnetic waves with a frequency range between 0.1 and 10 THz, and wavelengths approximately ranging from 0.03 to 3 mm, positioned between microwaves and infrared light in Fig. 1 [19, 20]. Due to its unique position in the electromagnetic spectrum,

the related theories are in a transitional region between macroscopic electromagnetism and microscopic photonics [21]. Compared to traditional light sources, THz waves possess unique advantages such as transient characteristics, low energy, high bandwidth, and coherence.

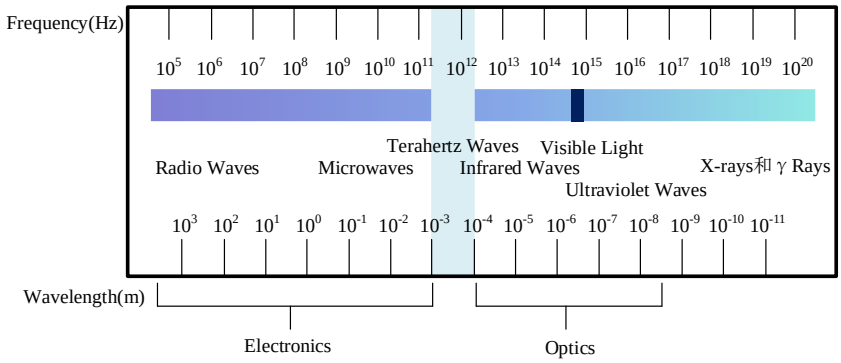

Fig. 1. Frequency and wavelength diagram of terahertz waves

According to Duvillaret and colleagues from the University of Savoy in France, an analytical method based on the Fresnel equations has been proposed, which can calculate the refractive index and extinction coefficient [22, 23]. The complex refractive index of the sample is expressed by the following formula:

$$\widetilde{n}(\omega) = \widetilde{n}(\omega) - jk(\omega). \tag{1}$$

Here $k(\omega)$ is the extinction coefficient, and $\eta(\omega)$ represents the real refractive index. In the THz transmission mode, the angle of incidence of the THz wave is perpendicular to the surface of the sample. According to the Fresnel equations, the transmission coefficient is expressed as:

$$R_{i,i+1}(\omega) = \frac{\widetilde{n}_{i+1}(\omega)\cos\theta - \widetilde{n}_i(\omega)\cos\beta}{\widetilde{n}_{i+1}(\omega)\cos\theta + \widetilde{n}_i\cos\beta}, \quad i = 0, 1, \tag{2}$$

$$T_{i,i+1}(\omega) = \frac{2\widetilde{n}_i(\omega)\cos\beta}{\widetilde{n}_{i+1}(\omega)\cos\theta + \widetilde{n}_i\cos\beta}, \quad i = 0, 1, \tag{3}$$

where: $R_{1,2}(\omega)$ represents the reflection coefficient at the interface between the silicone rubber and GFRP surface; $T_{1,2}(\omega)$ is the transmission coefficient between silicone rubber and GFRP; $R_{0,1}(\omega)$ is the reflection coefficient at the interface between air and silicone rubber; $T_{0,1}(\omega)$ is the transmission coefficient at the interface between air and silicone rubber; $\widetilde{n}_0(\omega)$ is the refractive index of air; $\widetilde{n}_1(\omega)$ is the refractive index of the first layer of silicone rubber; $\widetilde{n}_2(\omega)$ is the refractive index of the second layer of GFRP; θ is the angle of incidence; and β is the angle of refraction.

Let $E_0(\omega)$ represent the initial energy of the terahertz wave. In the model, the thicknesses of the silicone rubber and GFRP layers are d_1 and d_2, respectively; the distance between the terahertz emitter and the surface of the model is t_0; the thickness of the insulating layer is d_3; From the geometric relationship between t and d, the propagation distance of the terahertz wave in each medium layer is given by:

$$t_i = \frac{d_i}{\cos\beta_i}, \quad i = 1, 2, \tag{4}$$

where: t_1 and t_2 represent the propagation distances of the terahertz wave in silicone rubber and GFRP, respectively; β_1 and β_2 represent the angles of refraction of the terahertz wave in silicone rubber and GFRP, respectively.

The propagation factors of the terahertz wave in different media are given by:

$$P_i(\omega, t_i) = \exp\left[\frac{j\widetilde{n}_i(\omega)\,\omega t_i}{c}\right], \quad i = 0, 1, 2, \tag{5}$$

where: c is the speed of light; ω is the electromagnetic frequency of the terahertz wave; $P_0(\omega,t_0)$ is the propagation factor of the terahertz wave in air; $P_1(\omega, t_1)$ is the propagation factor of the terahertz wave in silicone rubber; $P_2(\omega, t_2)$ is the propagation factor of the terahertz wave in GFRP. silicone rubber and GFRP, respectively.

The propagation factors of the terahertz wave in different media are given by:

$$E_{r1}(\omega) = E_0(\omega) P_0(\omega, t_0)\, R_{01}. \tag{6}$$

The energy of the terahertz wave reflected after passing through the silicone rubber and reaching the surface of the GFRP is:

$$E_{r2}(\omega) = E_0(\omega) P_0^2(\omega, t_0)\, T_{01} P_1^2(\omega, t_1)\, R_{12} T_{10}, \tag{7}$$

where T_{10} represents the transmission coefficient between the first layer of the medium and air.

The energy of the reflected terahertz wave after passing through two layers of non-metallic media can be expressed as:

$$E_{r3'}(\omega) = E_0(\omega)\, P_0^2(\omega, l_0)\, T_{01}^2 P_1^2(\omega, l_1)\, T_{10}^2 P_0^2(\omega, l_a)\, R_{02}. \tag{8}$$

Therefore, the total energy received by the receiver after the terahertz wave is reflected by the layered defect structure is:

$$E_{R'}(\omega) = E_0 - E_{r1}(\omega) - E_{r2'}(\omega) - E_{r3'}(\omega) - E_m^*(\omega). \tag{9}$$

The use of dielectric discontinuity as a detection criterion is firmly grounded in Fresnel equations and electromagnetic boundary conditions. When terahertz waves encounter the GFRP-air interface at a fracture, the large dielectric constant mismatch creates strong reflection and transmission coefficient changes. Quantitative analysis shows:

1. Reflection coefficient $R \approx 0.36$ at the GFRP-air interface at normal incidence;
2. Corresponding transmission coefficient changes that directly affect the measured terahertz signal amplitude;
3. Theoretical prediction of energy contrast that matches our experimental observations. This electromagnetic theory demonstrates that dielectric discontinuity is a well-established physical mechanism for non-destructive testing, widely applied in terahertz detection of delamination and void defects in composites.

2.2. Preparation of experimental samples

This study employs flat GFRP specimens with material composition identical to actual core rods to establish fundamental understanding of terahertz-fracture interaction mechanisms under simplified geometric conditions. Extension to cylindrical geometries for practical field applications will require additional development including curved surface correction algorithms, cylindrical focusing optics, and potentially reflection-mode configurations. However, the fundamental frequency-domain and time-domain response characteristics identified in this work will remain applicable.

The experimental samples used in this study are composite insulators, which consist of a silicone rubber shed, a GFRP core rod, and metal fittings. As an important component in power systems, composite insulators serve the dual functions of providing electrical insulation and mechanical support. The basic structure of the composite insulator in Fig. 2, where the core rod is primarily made of epoxy resin and glass fiber composite material, offering high mechanical strength and good electrical insulation properties, while the metal fittings are used to connect the power lines to the composite insulator [24].

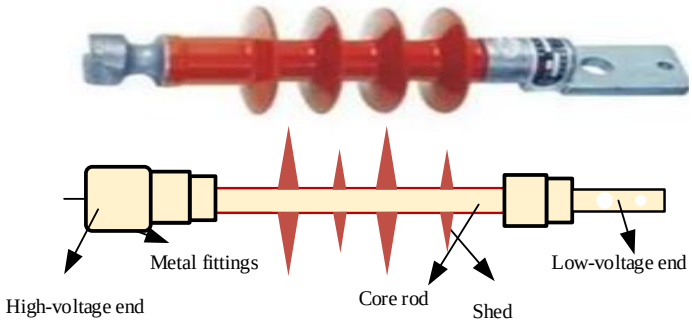

Fig. 2. Composite insulator structural diagram

The fracture defects in the core rod samples were created through controlled mechanical loading to simulate realistic brittle fracture failure modes. The samples contained transverse fracture defects in the GFRP core rod, representing complete separation with air gaps of approximately 0.5–2 mm width. This fracture pattern was selected because:

1) it represents the most critical structural failure mode requiring urgent detection;
2) the air-gap interface provides clear dielectric discontinuity for terahertz wave interaction;
3) this pattern corresponds to actual field failure cases documented in power systems.

The experimental samples are designed to simulate the fracture damage of composite insulators, with some of the core rods incorporating fracture defects. By artificially inducing fractures in the core rods, the impact of different types and shapes of fractures on terahertz wave propagation is studied. The design of these defected samples effectively simulates mechanical damage that may occur in real-world applications [25, 26]. The experimental test samples and measurement positions in Fig. 3, with three measurements taken for both the fractured and normal regions. Through the measurements of the experimental samples, the effect of core rod fractures on the terahertz wave propagation characteristics can be clearly observed, providing data support for the terahertz non-destructive testing method for internal defects in composite insulators.

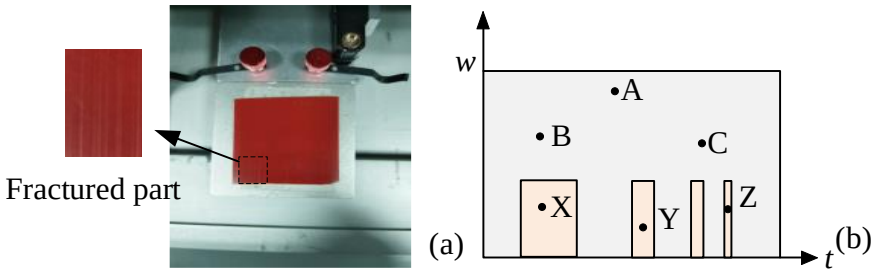

Fig. 3. Experimental fracture test samples and measurement positions: (a) complete sample overview showing fracture location; (b) detailed measurement positions where letters A, B, C indicate three measurement points in the fractured region, and D, E, F indicate three measurement points in the normal (non-fractured) region

2.3. Experimental methods and measurement equipment

This study uses a terahertz transmission-based high-resolution method to detect the samples, a technique capable of obtaining more detailed 'terahertz fingerprint spectra' features of the material. Figure 4 illustrates the working principle of the transmission-type THz-TDS system. In the experiment, the femtosecond laser pulse is split into two beams by a beam splitter: one beam serves as the pump light, which is directed onto the terahertz emitter after being adjusted by the time-delay system to generate broadband THz pulses; the other beam serves as the probe light, which, after merging with the THz pulse, enters the detector to simultaneously collect the time-domain signals [27]. By scanning the time delay, the waveform of the THz pulse electric field intensity as a function of time is obtained, and then Fourier transform is applied to obtain frequency-domain spectral information. Optical parameters such as transmittance and absorption coefficient of the sample are extracted, enabling quantitative comparative analysis of composite insulators in different interface states.

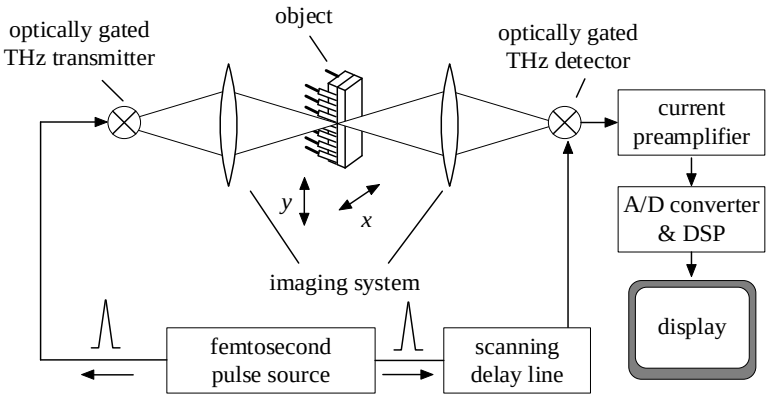

Fig. 4. Schematic principle of transmission-mode terahertz time-domain spectroscopy system, showing the beam path of pump and probe beams, terahertz generation and detection components, and sample positioning

This experiment employs a terahertz time-domain spectrometer (CCT-1800) system for non-destructive testing of the samples, with the testing principle in Fig. 5 and the instrumentation in Fig. 6. The core components of the system include a femtosecond laser, a terahertz wave emission and detection unit, and a time delay control system. The femtosecond laser, acting as the signal source, generates broadband terahertz radiation through ultrashort pulses, covering a frequency range from 0.1 THz to 2.5 THz, which effectively captures small defects in the internal structure of composite insulators. The main technical parameters are shown in Table 1 below:

Table 1. Test equipment parameters

Parameter	Value
Laser wavelength (nm)	780
Laser power (MW)	$50 \leq Ps \leq 80$
Laser pulse width (fs)	< 100
Spectral range (THz)	0.1–5
Peak dynamic range (dB)	≥ 90
Spectral resolution (GHz)	< 20
Scanning speed (scan/sec)	30
Experimental environment	15°C ~ 30°C, Nitrogen

The CCT-1800 THz-TDS system employs internal nitrogen purging of the emitter and detector modules to maintain dry atmosphere and optimize terahertz generation efficiency, while the sample chamber operates under ambient air conditions at controlled temperature (15–30°C) and relative humidity (typically < 50%). This distinction is important for understanding the measurement conditions and potential moisture effects on the results.

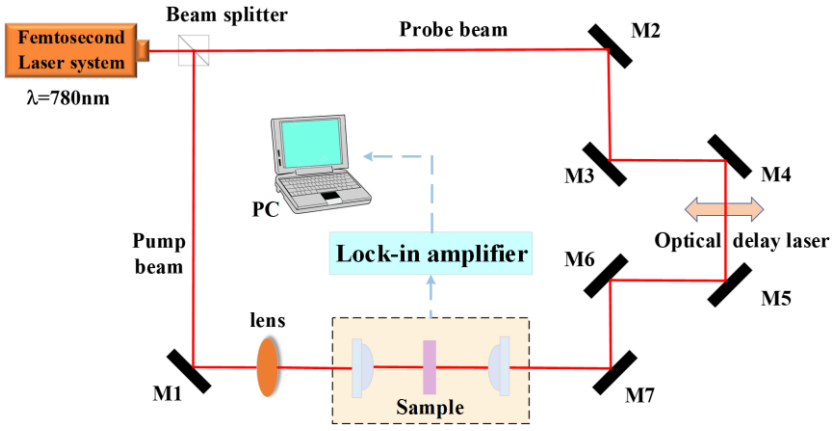

Fig. 5. Transmission-type THz-TDS system schematic, where M1-M7 represent parabolic mirrors for beam steering and focusing, the delay stage controls the relative timing between pump and probe pulses, and the sample is positioned in the terahertz beam path between the emitter and detector

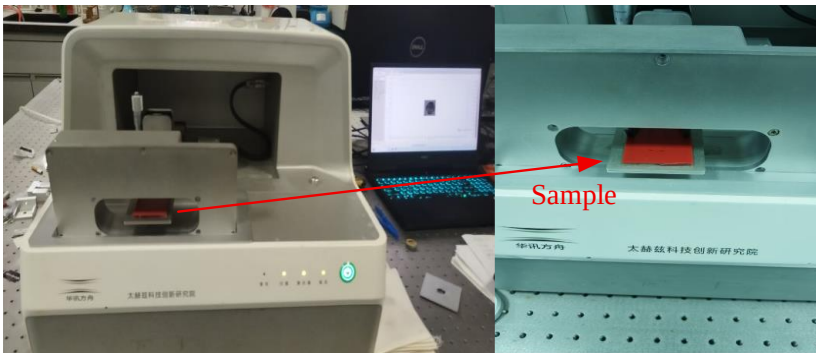

Fig. 6. THz-TDS testing device diagram and test sample

3. Experimental results and analysis

3.1. Terahertz imaging defect analysis

To visually demonstrate the response characteristics of the core rod fracture defect in the terahertz frequency range, this section employs frequency-domain imaging technology for three-dimensional spatial analysis of the test samples. By selecting two characteristic frequency points, 0.458 THz and 0.568 THz, imaging observations of the core rod fracture region are conducted from three perspectives: side view, top view, and front view. Figure 7 shows the frequency-domain imaging of the fracture regions at 0.458 THz and 0.568 THz, where the red areas in Fig. 7(a–f) represent the fracture regions. This approach comprehensively assesses the impact of the fracture defect on terahertz wave transmission. The comparative imaging analysis at different frequency points not only reveals the transmission energy variation caused by the medium discontinuity at the fracture, but also identifies the most sensitive characteristic frequencies for fracture boundary recognition, providing a foundation for subsequent quantitative defect evaluation.

The selection of 0.458 THz and 0.568 THz was based on systematic frequency-domain analysis of the entire 0.1–2.5 THz spectral range. Our analysis revealed that the 0.458 THz frequency exhibited maximum energy contrast between fractured and non-fractured regions, providing optimal sensitivity for defect detection and the 0.568 THz frequency was selected as a comparative reference point, showing different penetration depth and scattering characteristics. These frequencies fall within the high signal-to-noise ratio band of our CCT-1800 system, ensuring reliable measurements and the wavelengths corresponding to these frequencies provide appropriate balance between spatial resolution and penetration depth for GFRP materials. The imaging parameters used were: spatial resolution approximately 500 μm, scan step size 0.2 mm, and measurement time per point 0.5 seconds.

The frequency-domain images for the 0.458 THz and 0.568 THz frequency bands (Fig. 7). The red regions in the images highlight the fracture defects in the core rod of the composite insulator in the terahertz transmission detection. The intact core rod region allows terahertz waves to transmit normally, appearing as green regions with high transmission energy in the image. When the core rod fractures, the air gap and medium discontinuity formed at the fracture significantly

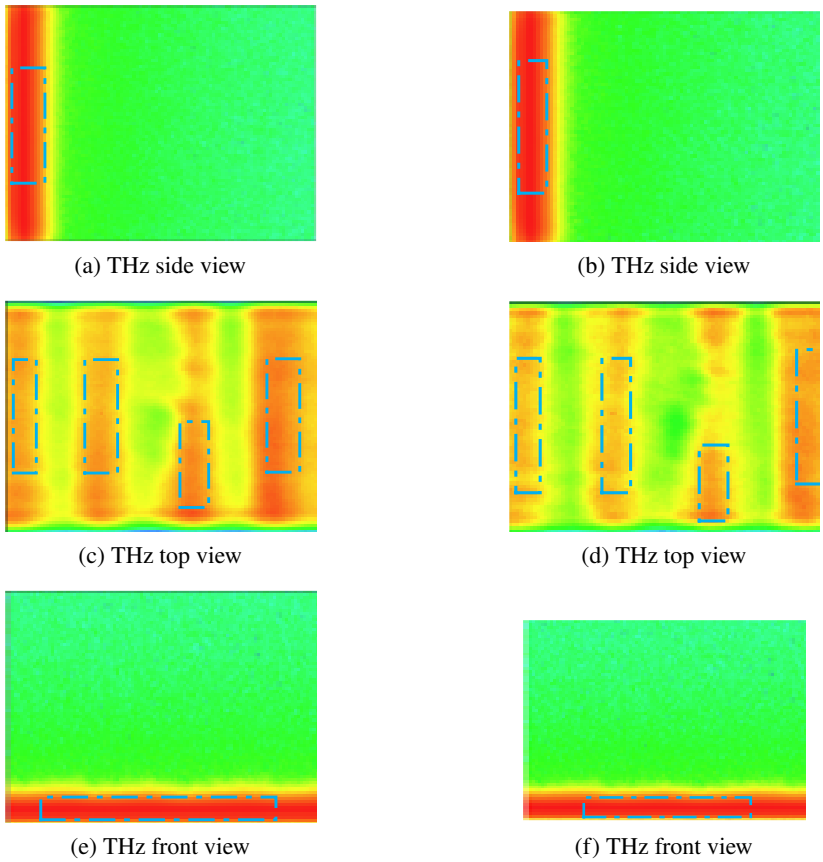

(a) THz side view (b) THz side view

(c) THz top view (d) THz top view

(e) THz front view (f) THz front view

Fig. 7. Multi-perspective terahertz transmission imaging of core rod fracture at two characteristic frequencies: (a) 0.458 THz lateral view imaging; (b) 0.458 THz axial view imaging; (c) 0.458 THz frontal view imaging; (d) 0.568 THz lateral view imaging; (e) 0.568 THz axial view imaging; (f) 0.568 THz frontal view imaging. Red regions indicate fractured areas with low THz transmission energy, while green regions indicate intact areas with high transmission energy

affect the terahertz wave transmission, leading to a substantial reduction in transmitted energy, which appears as red low-transmission regions in the frequency-domain image. A comparison between the 0.458 THz and 0.568 THz frequency bands reveals that 0.458 THz is more sensitive to the transmission energy variation at the fracture point, providing clearer fracture boundary identification. The red distribution in the Fig. 7(a), Fig. 7(b), and Fig. 7(c) regions of the image accurately reflect the fracture location in the core rod, where the air gap at the fracture blocks the normal transmission of terahertz waves, demonstrating the feasibility of using transmission-mode terahertz technology for identifying fractures in composite insulator core rods. It should be noted that the complex air gap structure at the fracture may cause scattering effects, leading to energy gradient changes around the red region, which could somewhat affect the precise evaluation of the fracture extent.

To accurately locate the core rod fracture region, further imaging was performed in the time domain using maximum peak imaging, minimum peak imaging, and peak-to-peak value imaging, with comparisons to the top view of the absorption spectrum imaging results. The test results using these four imaging modes in Fig. 8.

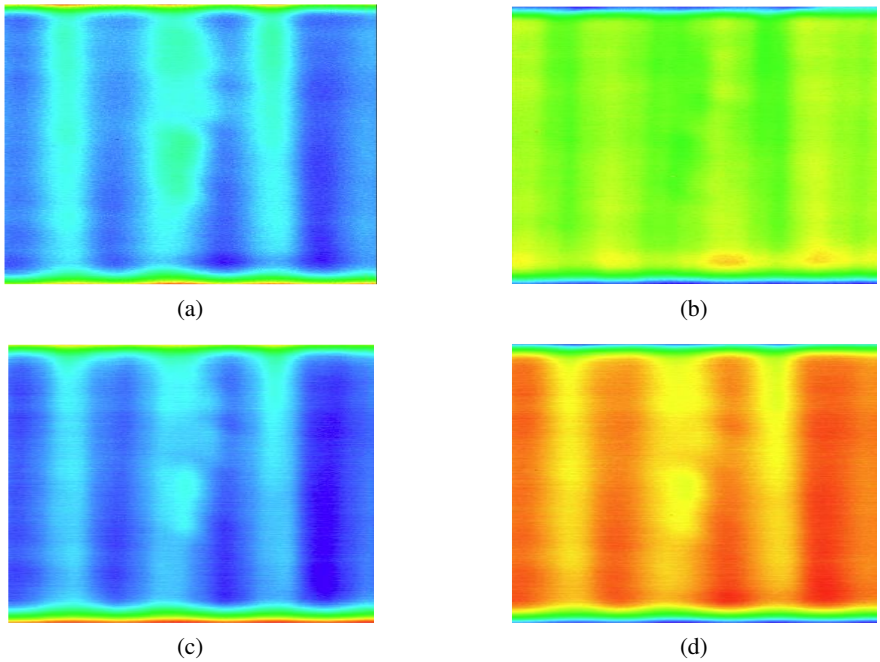

Fig. 8. (a) Absorption spectrum top view at 0.458 THz; (b) maximum peak imaging; (c) minimum peak imaging; (d) peak-to-peak value imaging

Based on the time-domain terahertz imaging results in Fig. 8, it can be observed that the time-domain characteristic parameters provide complementary diagnostic information to the frequency-domain analysis for core rod fracture defects. In the absorption spectrum top view at 0.458 THz Fig. 8(a), the fracture region exhibits significant changes in energy absorption characteristics, which corroborates the transmission energy reduction observed in the frequency-domain analysis, indicating that the medium discontinuity at the fracture not only affects the transmission properties but also alters the material's absorption response. Maximum peak imaging Fig. 8(b), minimum peak imaging Fig. 8(c), and peak-to-peak value imaging Fig. 8(d) reveal the time-domain response characteristics of the terahertz pulse in the fracture region from different perspectives: maximum peak imaging highlights the attenuation effect of the pulse peak at the defect, minimum peak imaging reflects baseline drift and scattering effects, while peak-to-peak value imaging comprehensively shows changes in the pulse dynamic range. Notably, the red-orange regions in the peak-to-peak value imaging Fig. 8(d) highly correspond to the fracture location in the frequency-domain image, indicating that the time-domain peak-to-peak value parameter can effectively quantify the terahertz waveform distortion at the fracture, providing reliable

time-domain feature-based evidence for the precise localization and severity assessment of core rod fractures in composite insulators. This, in turn, forms a complete multi-dimensional defect identification system in combination with frequency-domain transmission analysis.

3.2. Defect analysis of frequency-domain pulse waveform

The differences in frequency-domain responses between the normal region and the fracture defect region of composite insulators were analyzed, and three typical measurement points were selected in each region. The figure shows the frequency-domain energy spectra for both the normal and defect regions. It is clearly observed that the spectra of all samples almost completely overlap in the low-frequency region (below 0.1 THz) and the relatively high-frequency range (above 0.75 THz). However, as shown in Fig. 9, in the frequency range from 0.1 to 0.75 THz, the spectral differences between the two types of samples become significant, with the spectra of all defect samples being higher than those of the normal samples. This indicates that when a fracture defect occurs, the energy loss of the terahertz wave in the sample is reduced. The above test was repeated 15 times at other points, and the results were consistent. Therefore, selecting the frequency-domain spectrum within the 0.1–0.75 THz range can effectively identify whether a fracture defect has occurred inside the composite insulator, and can qualitatively analyze the presence of defects in practical applications.

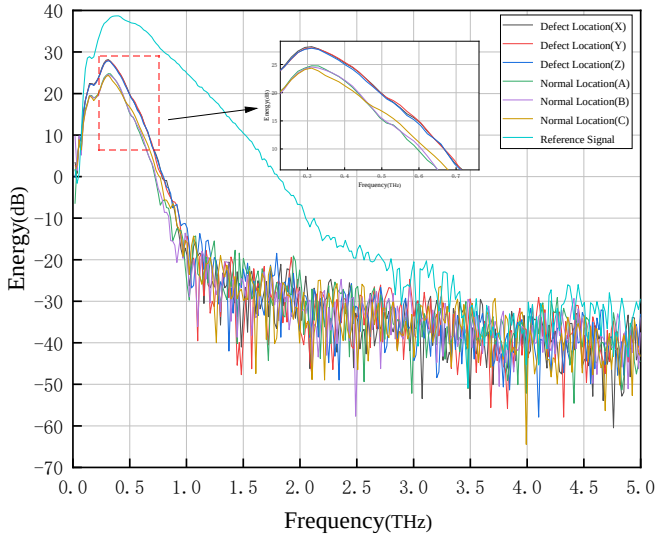

Fig. 9. Frequency-domain spectrum at different locations of the sample

3.3. Defect analysis of frequency-domain pulse waveform

To further analyze the fracture defects of the composite insulator, terahertz time-domain testing was conducted on the experimental samples.

Figure 10 compares the typical time-domain waveforms of the intact region Fig. 10(a) and the fracture region Fig. 10(b).

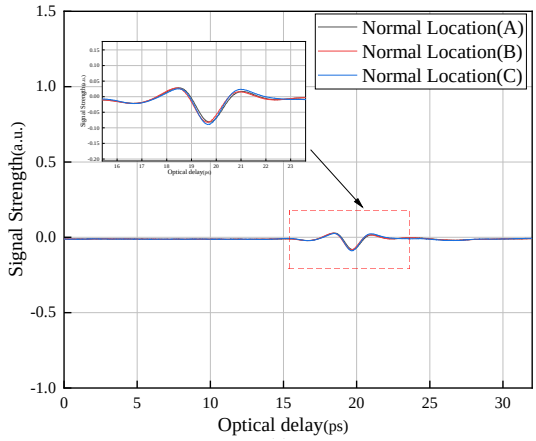

(a)

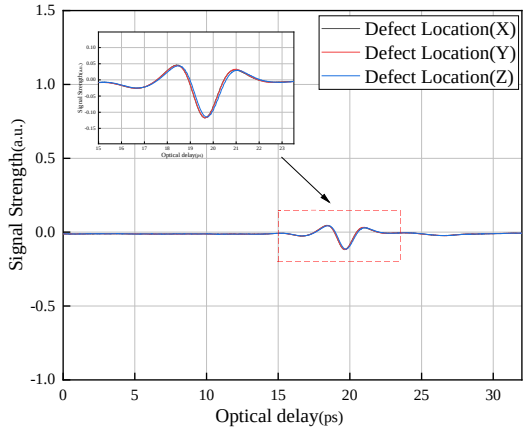

(b)

Fig. 10. (a) Time-domain waveform of the normal region; (b) time-domain waveform of the fracture defect region

There is a significant difference in the signal strength and amplitude variation of the negative peaks in the terahertz time-domain waveforms between the normal region and the fracture defect region. In the normal region, the negative peak has a smaller amplitude, and the waveform is generally smooth, indicating that the terahertz wave encounters less obstruction at the "silicone rubber–GFRP" interface, with relatively weak reflection. In the fracture defect region, the peak amplitude of the negative peak increases, accompanied by slight multiple reflection phenomena, suggesting stronger reflection and interference of the terahertz wave at the "silicone rubber–air–GFRP" interface. However, the extension of the wave's propagation path at the interface is not as prominent, and the increase in peak amplitude reflects enhanced energy scattering and loss. Therefore, by comparing the amplitude variation of the negative peak in the time-domain waveform, fracture defects inside the composite insulator can be intuitively and effectively identified and characterized.

From the above analysis, the presence of the fracture region increases the amplitude kurtosis of the time-domain spectrum. Composite insulators with different fracture degrees will exhibit changes in amplitude kurtosis due to the presence of air layers. Thus, the degree of fracture defects can be assessed by observing the changes in the amplitude kurtosis of the terahertz time-domain spectrum.

4. Conclusions

This study addresses the technical requirements for fracture detection in composite insulator core rods, and investigates a non-destructive identification method based on terahertz time-domain spectroscopy. Through theoretical analysis, experimental verification, and feature extraction, the following main conclusions are drawn:

1. The experimental results show that the dielectric discontinuity caused by core rod fractures generates significant frequency-domain response features during terahertz wave propagation. These differences can serve as qualitative criteria for identifying core rod fractures. In the effective identification frequency range of 0.1–0.75 THz, a systematic difference in the energy spectra between the fracture and normal regions is observed, with the transmission energy at the fracture consistently lower than that in the normal region. The stability and repeatability of the frequency-domain energy spectral differences were confirmed through repeated testing at multiple measurement points ($n = 15$), making it a reliable qualitative indicator for determining the presence of fractures in the core rod. This finding provides a theoretical foundation for developing a rapid screening method for composite insulators based on terahertz technology.
2. Through multi-frequency imaging and comparative analysis, 0.458 THz was determined to be the optimal characteristic frequency for fracture boundary identification, with its imaging contrast and boundary clarity significantly better than that of 0.568 THz. The frequency-domain imaging results align well with the time-domain peak-to-peak value imaging, with both methods mutually validating and enhancing the reliability of defect localization. Time-domain waveform analysis reveals that the negative peak amplitude increases in the fracture region and multiple reflection signals appear, reflecting the complex scattering behavior of terahertz waves at the fracture interface. The peak-to-peak value parameter effectively marks the spatial location of the fracture, providing an effective quantitative indicator for rapid field diagnosis.
3. Terahertz technology offers advantages such as non-contact, non-radiative, and high sensitivity, making it particularly suitable for detecting internal defects in composite materials. Experimental verification shows that the proposed detection method can effectively distinguish the normal region from the fracture region of the core rod, with clear and intuitive imaging results and reliable quantitative indicators. This technology provides core technical support for the development of intelligent monitoring systems for composite insulators, and has broad application prospects in the fields of equipment condition assessment and preventive maintenance in power systems.

Acknowledgements

This work was supported by the research and development project of State Grid Gansu Electric Power Company Electric Power Research Institute (No. 522722250002). The authors wish to thank the anonymous reviewers and editors for their valuable comments and contributions to the revision and finalization of this paper.

References

[1] Lv Y., Chen Z., Wang Q., Lu Y., Li X., *Simulation study on the structural optimization of composite insulators based on contaminant deposition*, Archives of Electrical Engineering, vol. 72, no. 4, pp. 1089–1105 (2023), DOI: 10.24425/aee.2023.147428.

[2] Yang S., Liu Y., Zhang B., Zhao Y., Ding H., *The Application of Terahertz Technology in Ultra High Voltage Large Tonnage Insulator Detection*, Energy Reports, vol. 9, pp. 128–141 (2023), DOI: 10.1016/j.egyr.2023.04.030.

[3] Koalla R., Chaudhary A.K., *Use of Effective Medium Theory for Characterization of Optical and Dielectric Properties of Explosive Composites in Terahertz Spectral Range*, Infrared Physics & Technology, vol. 151, 106129 (2025), DOI: 10.1016/j.infrared.2025.106129.

[4] Ukirade N.A., *A Review on Advancement of Materials for Terahertz Applications*, Next Materials, vol. 6, 100479 (2025), DOI: 10.1016/j.nxmate.2024.100479.

[5] Xu Y., Lian G., Zhou H., Hou Y., Zhang H., Zhang L., Chen X., *Terahertz Transfer Characterization for Composite Delamination Under Variable Conditions Based on Deep Adversarial Domain Adaptation*, Composites Science and Technology, vol. 232, 109853 (2023), DOI: 10.1016/j.compscitech.2022.109853.

[6] Guo Z., Sun Q., Li J., Deng L., Zhou T., Li Y., Deng L., *Nondestructive Detection on Defects of High-Voltage Polymeric Insulators with a RF/Microwave Patch Antenna*, Sensors and Actuators A: Physical, vol. 387, 116366 (2025), DOI: 10.1016/j.sna.2025.116366.

[7] Yuan C., Xie C., Li L., Zhang F., Gubanski S.M., *Ultrasonic Phased Array Detection of Internal Defects in Composite Insulators*, IEEE Transactions on Dielectrics and Electrical Insulation, vol. 23, no. 1, pp. 525–531 (2016), DOI: 10.1109/tdei.2015.005225.

[8] Tao Y.H., Fitzgerald A.J., Wallace V.P., *Non-Contact, Non-Destructive Testing in Various Industrial Sectors with Terahertz Technology*, Sensors, vol. 20, no. 3, 712 (2020), DOI: 10.3390/s20030712.

[9] Nsengiyumva W., Zhong S., Wang B., Zheng L., Zhang Z., Zhang Q., Peng Z., *Terahertz Spectroscopic Study of Optical and Dielectric Properties of Typical Electrical Insulation Materials*, Optical Materials, vol. 123, 111837 (2022), DOI: 10.1016/j.optmat.2021.111837.

[10] Li Y., Xie C., Gou B., Yu S., Yang C., *Terahertz Detection of Interface Defects Within Composite Insulators Using a Gated Recurrent Neural Network*, IEEE Transactions on Dielectrics and Electrical Insulation, vol. 31, no. 2, pp. 704–712 (2023), DOI: 10.1109/TDEI.2023.3330838.

[11] Kumosa M., Kumosa L., Armentrout D., *Causes and Potential Remedies of Brittle Fracture Failure of Composite (Nonceramic) Insulators*, IEEE Transactions on Dielectrics and Electrical Insulation, vol. 11, no. 6, pp. 1037–1048 (2005), DOI: 10.1109/TDEI.2004.1387827.

[12] Hu J., Liu W., Xie F., Xu S., Huang Z., Li W., *Study on Imaging Techniques and Quantitative Detection Method for Internal Void Defects in Rubber Based on Terahertz Reflection Imaging*, Optics Express, vol. 33, no. 7, pp. 15661–15681 (2025), DOI: 10.1364/OE.546988.

[13] Li S., Dan J., Yang D., Cui Y., Li T., Kang Y., Dong H., *Finite Difference Time Domain Modeling and Inversion of Internal Delamination Defects in Vehicle Cable Terminal in Terahertz Band*, IEEE Transactions on Instrumentation and Measurement, vol. 73, pp. 1–10 (2024), DOI: 10.1109/TIM.2024.3406831.

[14] Li S., Dan J., Geng T., Xue J., Kang Y., Dong H., *Terahertz Characterization of Cable Terminal: A Debye-PSO Modeling and Inversion Approach*, IEEE Transactions on Terahertz Science and Technology (2025), DOI: 10.1109/TTHZ.2025.3569133.

[15] Manoufali M., Naqvi S.A.R., Abbosh A.M., *Accurate Fourth-Order Debye Model for the Head Tissues Across the 0.1–1 GHz Band Using Metaheuristic Genetic Algorithm*, IEEE Journal of Electromagnetics, RF and Microwaves in Medicine and Biology, vol. 2, no. 2, pp. 79–86 (2018), DOI: 10.1109/JERM.2018.2809621.

[16] Wang J., Liang X., Gao Y., *Failure Analysis of Decay-Like Fracture of Composite Insulator*, IEEE Transactions on Dielectrics and Electrical Insulation, vol. 21, no. 6, pp. 2503–2511 (2015), DOI: 10.1109/TDEI.2014.004485.

[17] Jun Z., Hong Z., Wei L., *Research on the Remaining Life of Composite Insulator Silicon Rubber Skirt Based on Multi-Index Comprehensive Method*, Insulation Materials, pp. 1–10 (2025), DOI: 10.16790/j.cnki.1009-9239.im.2025.12.011.

[18] Guan Z., Lin Z., Run Z., Wen S., Xi L., *Status and Progress of Research on Aging Characterization and Evaluation of Silicon Rubber Composite Insulators*, High Voltage Apparatus, vol. 52, no. 4, pp. 1–15 (2016), DOI: 10.13296/j.1001-1609.hva.2016.04.001.

[19] Xi L., Yan G., *Study on Brittle Fracture of Composite Insulators (Part 1): Main Characteristics, Definitions, and Criteria of Brittle Fracture*, CSEE Journal of Power and Energy Systems, vol. 36, no. 17, pp. 4778–4786 (2016), DOI: 10.13334/j.0258-8013.pcsee.160490.

[20] Yan G., Xi L., *Study on Brittle Fracture of Composite Insulators (Part 2): Experimental Simulation and Discussion on Preventive Measures for Brittle Fracture*, CSEE Journal of Power and Energy Systems, vol. 36, no. 18, pp. 5070–5077+5132 (2016), DOI: 10.13334/j.0258-8013.pcsee.160491.

[21] Zhong Z., Hong M., Jian L., Wang W., Li W., Lan L., Huai J., Guang Y., *Research on Interface Detection of Composite Insulators Based on Terahertz Waves*, CSEE Journal of Power and Energy Systems, vol. 40, no. 3, pp. 989–999 (2020), DOI: 10.13334/j.0258-8013.pcsee.190699.

[22] Zhi T., Yang L., *Review of Terahertz Reflection Imaging Technology in the Detection of Internal Defects in Composite Insulator Silicone Rubber*, Insulation Materials, vol. 55, no. 7, pp. 10–16 (2022), DOI: 10.16790/j.cnki.1009-9239.im.2022.07.002.

[23] Li S., Cao B., Cui Y., Kang Y., Gao S., Li H., Dong H., *Terahertz-Based Insulation Delamination Defect Inspection of Vehicle Cable Terminals*, IEEE Transactions on Transportation Electrification, vol. 9, no. 1, pp. 1765–1774 (2022), DOI: 10.1109/TTE.2022.3200043.

[24] Li S., Li T., Jia D., Yong Q., Hai D., *Review on Terahertz Non-Destructive Testing of Composite Insulation Structures in Electrical Equipment*, High Voltage Engineering, vol. 50, no. 1, pp. 194–209 (2024), DOI: 10.13336/j.1003-6520.hve.20232250.

[25] Liu Y., Guo Y., Fan Y., Zhou J., Li Z., Xiao S., Wu G., *Optical Imaging Technology Application in Transmission Line Insulator Monitoring: A Review*, IEEE Transactions on Dielectrics and Electrical Insulation, vol. 31, no. 6, pp. 3120–3132 (2024), DOI: 10.1109/TDEI.2024.3351093.

[26] Zou Z., Qiu H., Wang Z., Liu Z., Kuang C., *An Ultrasonic Phased Array Method for Detecting the Internal Defects in Composite Insulators by Using the Concave Probe*, IEEE Transactions on Dielectrics and Electrical Insulation, vol. 32, no. 1, pp. 541–550 (2024), DOI: 10.1109/TDEI.2024.3481364.

[27] Hong M., Huai J., Jian L., Da C., Li W., Li W., *Terahertz Imaging Method for Composite Insulator Defects Based on Edge Detection Algorithm*, IEEE Transactions on Instrumentation and Measurement, vol. 43, no. 5, pp. 2029–2040 (2023), DOI: 10.1109/TIM.2021.3075031.